The Bell System Technical Journal
Vol. 52, No. 5, May–June, 1973
Printed in U.S.A.

The Potential in a Charge Coupled Device With No Mobile Minority Carriers And Zero Plate Separation

By J. McKENNA and N. L. SCHRYER

(Manuscript received November 1, 1972)

A two-dimensional analysis of the potential in charge coupled devices is presented. It is assumed that there are no mobile minority carriers, that the plate separation is zero, and that the plate voltage does not vary with time. The depletion layer approximation is used to linearize the equations, which are then solved exactly with the use of Fourier series. Both surface and buried channel devices are analyzed. These solutions can typically be evaluated on a computer in less than a tenth of the time it takes to obtain a solution by the method of finite differences. The solutions obtained here provide an important tool for the designer of charge coupled devices. In addition to describing the method of obtaining the solutions, we evaluate them to show the effects of a number of different design parameters, and compare the cost of these solutions with the cost of obtaining finite difference solutions.

1. INTRODUCTION AND SUMMARY

The recent invention[1,2] and development of charge coupled devices (CCD's) has led to renewed interest in the mathematical analysis of MIS-type structures. Ideally, one would like to solve the nonlinear equations describing the three-dimensional motion of charge as a function of the time-varying plate voltages. So far no one has succeeded in doing this for even the simplest geometries. For the most part, one-dimensional static models have been solved which yield only qualitative information about the behavior of such devices. A much more sophisticated, one-dimensional, time-varying model of a CCD has been developed and analyzed by Schryer and Strain.[3]

A static, two-dimensional model of a CCD has also been studied by Amelio[4] using finite difference techniques. He calculated the potential distribution in a two-dimensional model in the absence of mobile

charge and with given static plate potentials. The results of this calculation are of great interest. The use of finite difference techniques in these cases has drawbacks, however. In even the relatively simple geometries considered so far, it is expensive to obtain reasonably accurate solutions for the potentials, and for more complicated devices, it soon becomes prohibitively expensive. Furthermore, as we shall show, even for simple geometries it is difficult to obtain accurate expressions for the fields from the finite difference solutions for the potentials.

In this paper, we show that when the plates on a CCD are close enough together so that they can be assumed to be abutted, and when the depletion layer approximation can be used,[5] the resulting linearized model can be solved analytically. These solutions can then be evaluated cheaply and quickly on a computer. This analysis will be valid for both surface and buried channel CCD's with an arbitrary number of plates. In a separate paper, we will show that these solutions can be used to obtain solutions for the potential in a CCD when there are gaps between the plates.[6]

In Section II we write down the equations describing the model and put them into appropriate dimensionless form. We then introduce the depletion layer approximation which linearizes the equations and discuss conditions under which this approximation is valid.

This paper has two main purposes: to show the behavior of the potentials and fields in a CCD and to demonstrate techniques by which these potentials and fields can be calculated cheaply and accurately. In Section III we present a discussion of how the solutions depend on the various parameters defining the devices.

In Section IV we derive the solution of the linearized potential equations. The reader interested only in the physical design of CCD's can skip the rest of the paper.

In Section V we discuss in some detail the solution by finite difference methods of the exact, nonlinear equations describing a surface CCD. Our purpose in doing this is twofold. We wish to show the difficulties involved in obtaining an accurate solution cheaply, especially if an accurate knowledge of the fields is required. Secondly, we want accurate solutions of the exact problem to compare with the analytic solutions of the linearized problem.

Finally, in Section VI we compare in detail some solutions of the exact problem obtained by finite differences with the corresponding analytic solutions of the linearized equations. It is shown that in many cases of interest the solutions of the linearized problem provide excel-

lent approximations to the true potential and much more accurate approximations to the gradient of the potential than can be obtained from the finite difference solutions. Furthermore, the solutions of the linearized equations are at least an order of magnitude cheaper to obtain than are the finite difference solutions for any reasonable accuracy.

II. DERIVATION OF THE EQUATIONS

A surface CCD[1] consists of a layer of silicon covered with a thin insulating layer of silicon dioxide, and on top of the oxide layer, a sequence of closely spaced electrodes. Such a device is shown schematically in Fig. 1 with some typical dimensions indicated. Mobile charge trapped at the oxide-semiconductor interface is transferred from plate to plate by appropriately changing the potential of the plates. We consider the case where the substrate is n-type silicon and the mobile charges are injected holes. In this case, the plate potentials must be negative. Our analysis can be modified in an obvious way to describe the case where the substrate is p-type silicon and the mobile charges are electrons.

Some losses are introduced by the trapping of the mobile charges by surface states at the oxide-semiconductor interface. Smith and Boyle[7,8] have proposed a solution to this problem by inserting between the oxide and the substrate an additional layer of p-type silicon, thus forming a buried channel CCD. The p-layer is kept completely ionized, which

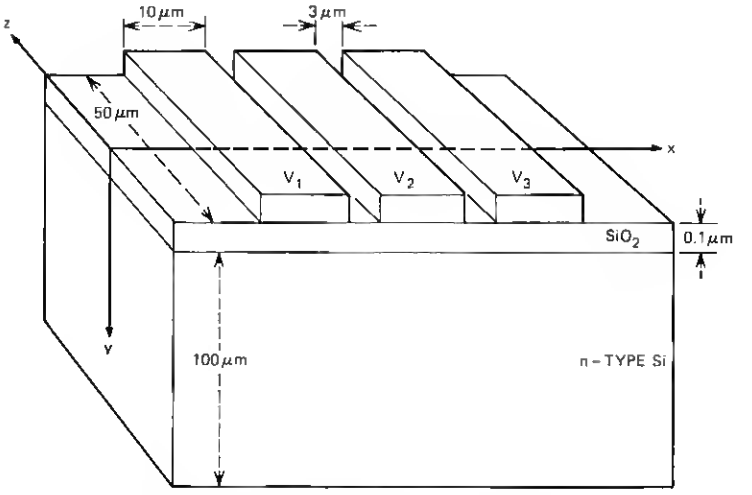

Fig. 1—A schematic diagram of a surface CCD.

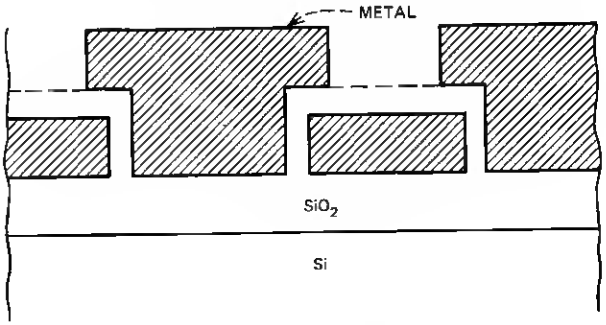

Fig. 2—A schematic diagram illustrating plate overlap structure.

causes the potential minimum to occur near the center of the p-layer. Thus the mobile positive charge stays at the potential minimum, safely away from the surface traps.

It is desirable to have tbe plates as close together as possible in order to minimize the transit time of the mobile charge between plates. The minimum plate separation presently obtainable from photolithography is ~3–5 μm, but a plate overlap structure,[8,9] as shown in Fig. 2, or undercut isolation[10] allows for plate separation of ~0.1 μm.

We propose to study the static potential in either a surface or buried channel CCD with plate overlap structure, in the absence of mobile charge. We begin by noting that since the length in the z-direction of each plate is much greater than its width in the x-direction, near the center of the plates ($z = 0$) the field is essentially two-dimensional. Hence we will treat the problem as two-dimensional. We assume that the plates are zero distance apart. Since in the overlap structure there sbould be little flux leakage between the plates, we feel this is a reasonable approximation. We make the additional assumption that the bottom substrate is infinitely thick. The field can penetrate into tbe substrate little beyond a depletion depth, and since for typical voltages the depletion depth ranges from 7 μm to 20 μm, and the thickness of tbe substrate in a typical device is 100 μm, this is a very reasonable approximation. Finally, we assume tbe structure is periodic in the x-direction, which in the usual mode of operation is an excellent approximation.

We begin by defining the boundary value problem describing a buried channel device. In all that follows, starred quantities have rationalized MKS dimensions; unstarred quantities, except for a few obvious physical parameters, are dimensionless. In tbe strip $0 \leqq x^* \leqq L^*$, let φ_1^* denote the potential in the oxide layer, $0 \leqq y^* \leqq h_1^*$; φ_2^* the potential in the p-layer, $h_1^* \leqq y^* \leqq h_2^*$; and φ_3^* the po-

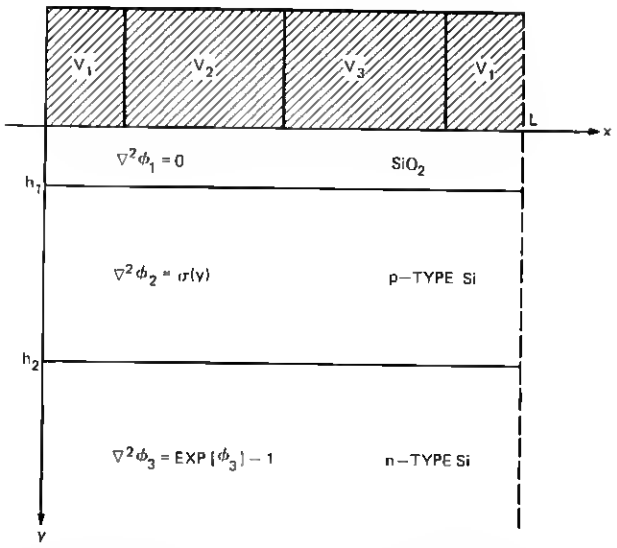

Fig. 3—A schematic diagram of one cell of a three-phase, buried channel CCD.

tential in the substrate, $h_2^* \leqq y^* < \infty$ (see Fig. 3). Then

$$\nabla_*^2 \varphi_1^* = 0, \tag{1}$$

$$\nabla_*^2 \varphi_2^* = \frac{e}{\epsilon_2} N_A^*(y^*) \tag{2}$$

$$\nabla_*^2 \varphi_3^* = -\frac{eN_D^*}{\epsilon_2}(1 - \exp(e\varphi_3^*/kT)). \tag{3}$$

In eqs. (1) through (3), ∇_*^2 is the two-dimensional Laplacian; $-e$ is the charge of an electron; $N_A^*(y^*)$ is the acceptor number density in the p-region; N_D^* is the donor number density in the n-region; ϵ_1 and ϵ_2 are the permittivity of the oxide and silicon, respectively; k is Boltzman's constant; and T is the absolute temperature. The conditions under which eq. (3) can be expected to be valid are discussed in Ref. 11.

In the usual method of fabricating a CCD, the substrate donor number density, N_D^*, is a constant, independent of position. However, in a buried channel CCD, the p-layer is formed by diffusing the acceptor ions into the n-type Si, and so $N_A^*(y^*)$ is typically a function of $y^* - h_1^*$, the distance from the oxide surface. In many cases we have the representation[12]

$$N_A^*(y^*) = C_S^* \exp\left\{-\left(\frac{y^* - h_1^*}{h_2^* - h_1^*}\right)^2 \ell n \frac{C_S^*}{N_D^*}\right\} - N_D^* \tag{4}$$

where C_S^* is the number density of acceptor ions at the upper surface of the Si. The average value, $\bar{N}_A^*$, of $N_A^*(y)$ is easily shown to be

$$\bar{N}_A^* = \frac{1}{h_2^* - h_1^*} \int_{h_1^*}^{h_2^*} N_A(y^*) dy^*$$

$$= \frac{\sqrt{\pi}}{2} \frac{C_S^*}{\sqrt{\ell n(C_S^*/N_D^*)}} \operatorname{erf} \left(\sqrt{\ell n(C_S^*/N_D^*)}\right) - N_D^* \tag{5}$$

where erf (x) is the error function.[13]

Before writing down the boundary conditions, we introduce dimensionless variables. Define the Debye length

$$\lambda_D = (\epsilon_2 \mathrm{k}T/e^2 N_D^*)^{\frac{1}{2}}. \tag{6}$$

Then normalize all lengths with respect to λ_D,

$$\begin{gathered} x = x^*/\lambda_D, \qquad y = y^*/\lambda_D, \qquad L = L^*/\lambda_D, \\ h_k = h_k^*/\lambda_D, \qquad (k = 1, 2), \end{gathered} \tag{7}$$

and define

$$\varphi_\alpha(x, y) = e\varphi_\alpha^*(x^*, y^*)/\mathrm{k}T, \qquad (\alpha = 1, 2, 3), \tag{8}$$

$$\sigma(y) = N_A(y^*)/N_D^*, \qquad \eta = \epsilon_1/\epsilon_2. \tag{9}$$

Equations (1) through (3) become

$$\nabla^2 \varphi_1 = 0, \tag{10}$$

$$\nabla^2 \varphi_2 = \sigma(y), \tag{11}$$

$$\nabla^2 \varphi_3 = e^{\varphi_3} - 1. \tag{12}$$

The boundary conditions can be written now as follows: For $0 \leqq x \leqq L$,

$$\varphi_1(x, 0) = V(x), \tag{13}$$

$$\varphi_1(x, h_1) = \varphi_2(x, h_1), \quad \eta \frac{\partial \varphi_1}{\partial y}(x, h_1) = \frac{\partial \varphi_2}{\partial y}(x, h_1) + Q(x), \tag{14}$$

$$\varphi_2(x, h_2) = \varphi_3(x, h_2), \quad \frac{\partial \varphi_2}{\partial y}(x, h_2) = \frac{\partial \varphi_3}{\partial y}(x, h_2), \tag{15}$$

$$\varphi_3(x, \infty) = 0, \tag{16}$$

and

$$\begin{aligned} \varphi(0, y) &= \varphi(L, y) \\ \frac{\partial \varphi}{\partial x}(0, y) &= \frac{\partial \varphi}{\partial x}(L, y), \qquad 0 \leqq y < \infty. \end{aligned} \tag{17}$$

In (13), $V(x)$ is a given, periodic function, assuming on each electrode the constant voltage of the electrode; and in (14), $Q(x)$ is a known,

periodic surface charge density, which may include deliberately implanted charges.[14]

For future use, we record the expression for $\sigma(y)$ when $N_A(y^*)$ is given by (4). If

$$C_S = C_S^*/N_D^*, \tag{18}$$

then

$$\sigma(y) = C_S \exp\left\{-\left(\frac{y - h_1}{h_2 - h_1}\right)^2 \ell n C_S\right\} - 1, \tag{19}$$

and

$$\bar{\sigma} = \frac{\sqrt{\pi}}{2} \frac{C_S \operatorname{erf}(\sqrt{\ell n C_S})}{\sqrt{\ell n C_S}} - 1. \tag{20}$$

The equations for the surface CCD are essentially the same, except that the p-layer is eliminated. In what follows, we will only give the analysis for the buried channel CCD. The results for the surface CCD can be obtained from those for the buried channel CCD by setting $\sigma = 0$, $h_1 = h_2$, and $\varphi_3 = \varphi_2$.

We now introduce the important depletion layer approximation.[5]

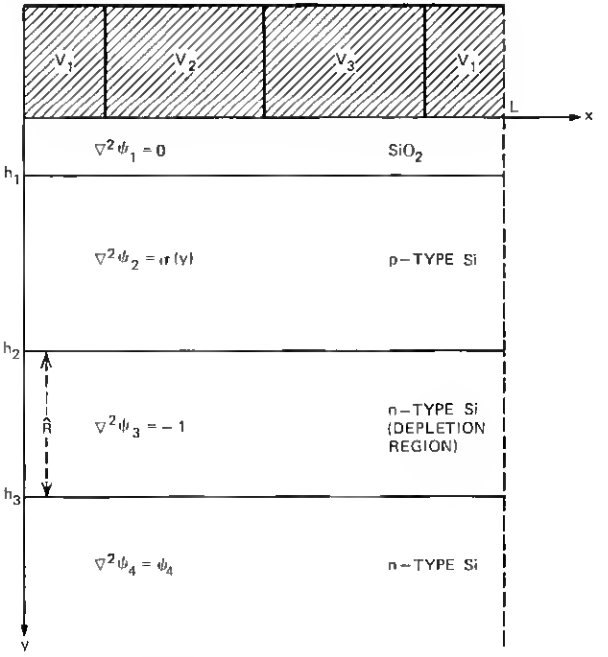

Fig. 4—A schematic diagram of the depletion layer approximation for one cell of a three-phase, buried channel CCD.

In most cases of interest, $\varphi_3(x, h_2) \ll -1$ for $0 \leqq x \leqq L$. For example, in a typical buried channel CCD, $\varphi_3(x, h_2) \sim -1000$ [and in a typical surface CCD, $\varphi_2(x, h_1) \sim -150$]. Thus, for $y - h_2$ small and positive, $e^{\varphi_3} \sim 0$. However, for $y \gg h_2$, $|\varphi_3| \ll 1$, and $e^{\varphi_3} \cong 1 + \varphi_3$. There is thus some curve $y = R(x)$ such that for $h_2 \leqq y \leqq R(x)$, $e^{\varphi_3} - 1 \approx -1$. The region $h_2 \leqq y \leqq R(x)$ is the depletion region. For $R(x) < y$, we have $e^{\varphi_3} - 1 \sim \varphi_3$. If $R(x)$ varies but little about its average value, $\hat{R}$, these remarks suggest that we replace eqs. (10) through (12) by the system of linear equations

$$\nabla^2\psi_1(x, y) = 0, \qquad 0 < y < h_1, \tag{21}$$

$$\nabla^2\psi_2(x, y) = \sigma(y), \qquad h_1 < y < h_2, \tag{22}$$

$$\nabla^2\psi_3(x, y) = -1, \qquad h_2 < y < h_3 = h_2 + \hat{R}, \tag{23}$$

$$\nabla^2\psi_4(x, y) = \psi_4(x, y), \qquad h_3 = h_2 + \hat{R} < y < \infty \tag{24}$$

where ψ_3 is the potential in $h_2 \leqq y \leqq h_3$ and ψ_4 is the potential in $h_3 \leqq y < \infty$. (See Fig. 4.) In addition to ψ_1, ψ_2, and ψ_3 satisfying boundary conditions (13) through (15), we have the boundary conditions, for $0 \leqq x \leqq L$,

$$\psi_3(x, h_3) = \psi_4(x, h_3), \qquad \frac{\partial\psi_3}{\partial y}(x, h_3) = \frac{\partial\psi_4}{\partial y}(x, h_3), \tag{25}$$

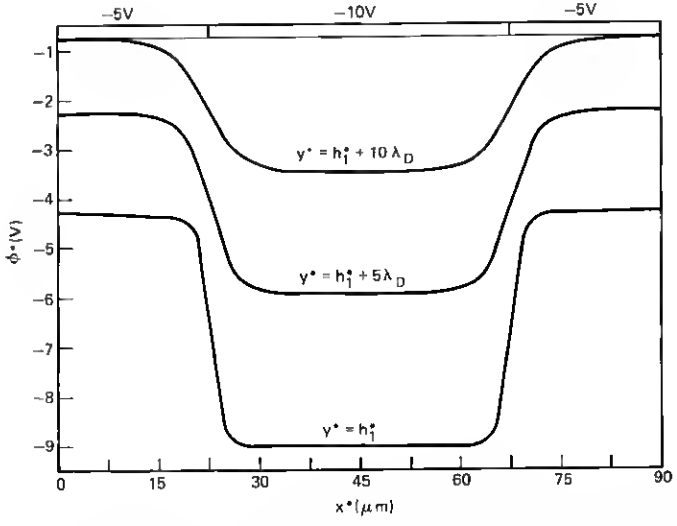

Fig. 5—The potential $\varphi^*(x^*, y^*)$ plotted as a function of x^* in a surface CCD for $y^* = 0.2$ μm, 2.275 μm, and 4.35 μm. The 45-μm plates are alternately at -5 V and -10 V, and the oxide thickness is $h_1^* = 0.2$ μm.

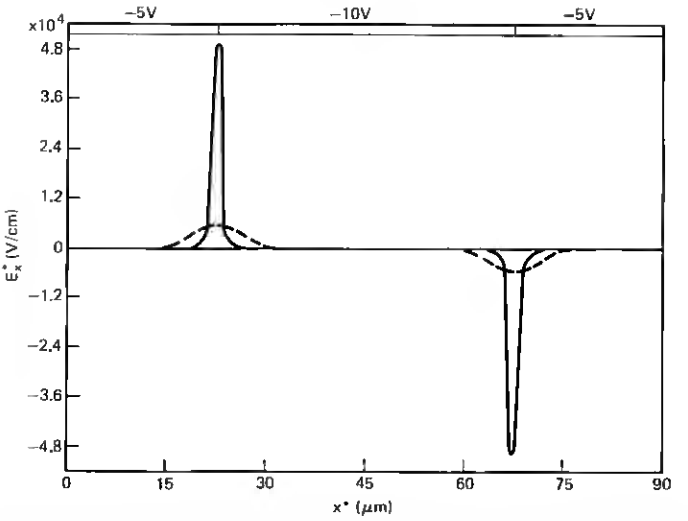

Fig. 6—The field $-(\partial\varphi^*/\partial x^*)(x^*, y^*)$ plotted as a function of x^* in a surface CCD for $y^* = 0.2$ μm. The 45-μm plates are alternately at −5 V and −10 V, and the oxide thickness is $h_1^* = 0.2$ μm. The dashed curve is a plot of $-(\partial\varphi^*/\partial x^*)$ for the same device obtained from a finite difference calculation.

$$\psi_4(x, \infty) = 0, \tag{26}$$

and the ψ_α ($\alpha = 1, 2, 3, 4$) all satisfy (17).

It has been shown that for a one-dimensional version of this problem, the choice[5]

$$\hat{R} = -\left(1 + h_2 - h_1 + \frac{h_1}{\eta}\right) + \left[\left(h_2 - h_1 + \frac{h_1}{\eta}\right)^2 - 1 - 2V_o - \frac{2h_1}{\eta} Q_{ss} + 2\int_{h_1}^{h_2}\left(\xi - h_1 + \frac{h_1}{\eta}\right)\sigma(\xi)d\xi\right]^{\frac{1}{2}} \tag{27}$$

yields a solution which approximates the solution of the nonlinear problem very accurately in the region $h_1 \leqq y \leqq h_2$. Furthermore, the solution in this region is quite insensitive to the choice of $\hat{R}$. Since an accurate knowledge of the potential is only necessary in the p-layer for the buried channel CCD and near the oxide-semiconductor interface for the surface CCD, we feel this approximation is well justified. In this two-dimensional problem, we determine $\hat{R}$ from (27) by letting V_o and Q_{ss} be the averages of $V(x)$ and $Q(x)$:

$$V_o = \frac{1}{L}\int_0^L V(x)dx, \qquad Q_{ss} = \frac{1}{L}\int_0^L Q(x)dx. \tag{28}$$

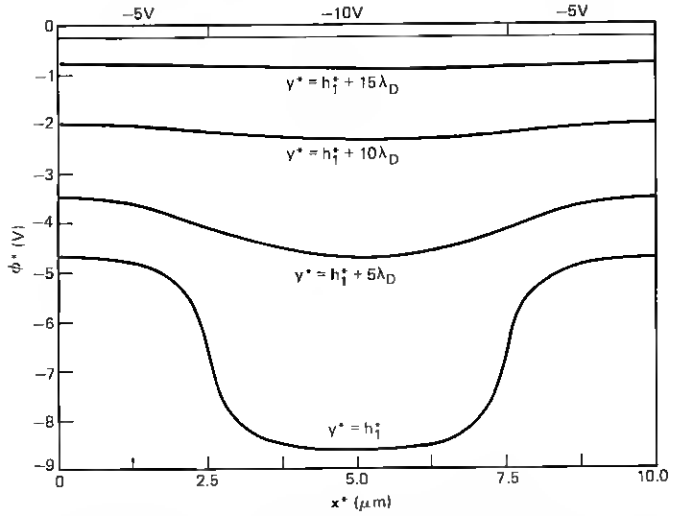

Fig. 7—The potential $\varphi^*(x^*, y^*)$ plotted as a function of x^* in a surface CCD for $y^* = 0.2$ μm, 2.275 μm, 4.35 μm, and 6.425 μm. The 5-μm plates are alternately at -5 V and -10 V, and the oxide thickness is $h_1^* = 0.2$ μm.

In Section VI we will present a comparison of the solution of the linearized equations with the solution of the nonlinear equations obtained by finite difference methods. This will confirm for this example that the approximate solutions are accurate as claimed.

III. GENERAL BEHAVIOR OF THE POTENTIALS AND FIELDS

In this section we present graphical representations of the potentials and fields for both surface and buried channel CCD's for a number of design parameters. The graphs were obtained by evaluating the analytic expressions for the solutions, derived in Section IV, of eqs. (13) through (15), (17), and (21) through (26).

In all cases, we assume that the doping in the n-type substrate is $N_D = 10^{14}/\text{cm}^3$, that $\epsilon_2/\epsilon_0 = 12$, where ϵ_0 is the permittivity of free space, that $\epsilon_1/\epsilon_2 = \frac{1}{3}$, and that $Q(x) \equiv 0$, i.e., there is no trapped or implanted charge at the semiconductor-oxide interface. Then at $T = 300°\text{K}$, the value of λ_D defined in (6) is $\lambda_D = 4.15 \times 10^{-5}$ cm. Also, in all the examples presented here, we have used the factor $(kT/e) = 0.025$ V to convert dimensionless potentials to volts, and the factor $(kT/e\lambda_D) = 600$ V/cm to convert dimensionless fields to V/cm.

We consider first the effect of plate width in surface devices. The first pair of graphs illustrate a surface CCD with 45-μm plates, the second

pair a surface CCD with 5-μm plates, and the third pair a surface CCD with 1.5-μm plates. The oxide layer in each of these CCD's is 0.2 μm thick, and the voltages on the plates are alternately -5 V and -10 V. These examples show the storage mode, and as a result there is no asymmetry to introduce a perferred direction of flow for the holes. However, they do exhibit the effects of plate width, and are easy to compare with finite difference calculations. In Figs. 5, 7, and 9, φ^* is plotted along the oxide-semiconductor interface ($y^* = h_1^*$) and along the lines $y^* = h_1^* + 5\lambda_D$, $h_1^* + 10\lambda_D$, and $h_1^* + 15\lambda_D$ inside the substrate. In Figs. 6, 8, and 10, $-(\partial\varphi^*/\partial x^*) = E_x^*$ is plotted along the oxide-semiconductor interface. The dashed curve is the field calculated by finite difference methods. The discrepancy between the two curves will be discussed in Section V.

In all three cases, the peak field available for moving positive charge from the left-hand plate to the center plate is about 4.8×10^4 V/cm. However, in the 45-μm plate device, the field penetrates only about 7 μm under the plate from the edge, leaving most of the region under the plate field free. This would clearly be a very poor CCD. On the other hand, in the 1.5-μm device, there are substantial fields under the whole plate. These graphs show that if field penetration under the plates were the sole criterion, the narrower the plates the better. How-

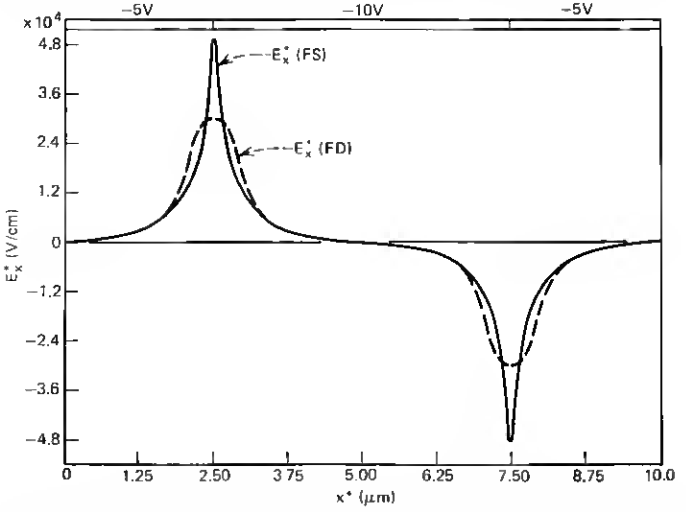

Fig. 8—The field $-(\partial\varphi^*/\partial x^*)(x^*, y^*)$ plotted as a function of x^* in a surface CCD for $y^* = 0.2$ μm. The 5-μm plates are alternately at -5 V and -10 V, and the oxide thickness is $h_1^* = 0.2$ μm. The dashed curve is a plot of $-(\partial\varphi^*/\partial x^*)$ for the same device obtained from a finite difference calculation.

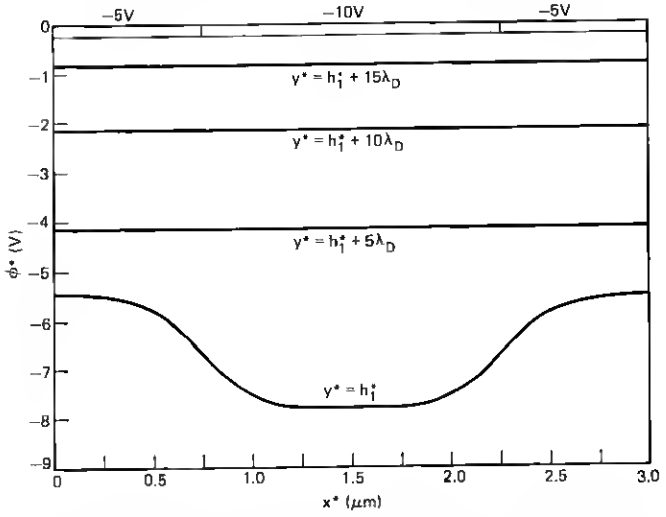

Fig. 9—The potential $\varphi^*(x^*, y^*)$ plotted as a function of x^* in a surface CCD for $y^* = 0.2$ μm, 2.275 μm, 4.35 μm, and 6.425 μm. The 1.5-μm plates are alternately at −5 V and −10 V, and the oxide thickness is $h_1^* = 0.2$ μm.

ever, recent work by Tompsett[15] has shown that in surface CCD's the difference in losses of ones and fat zeros due to surface states becomes greater as the plate width decreases. His work shows that this puts a lower bound on plate widths in the neighborhood of 5 μm. However, Fig. 8 shows that for 5-μm plates there is still considerable field penetration under the plates.

Our calculations show that increasing (decreasing) the thickness of the oxide layer decreases (increases) the peak values of the fields, but does not materially affect the penetration of the fields under the plates.

We next consider buried channel CCD's. As for surface devices in general, the narrower the plates the better as far as field penetration is concerned. However, the plate width is apt to be determined by current photolithography tolerances, so this is a parameter not easily varied. In addition, if the plates are too narrow, the charge-carrying capacity of the CCD becomes very small.

Instead of considering the effects of plate width, we examine what happens for a given plate width if the thickness of the p-type layer is varied. We consider first a three-phase, buried channel CCD with 5-μm plates. The plates are at −5 V, −10 V, and −15 V, so charge is to be moved from under the −10 V plate to under the −15-V plate. The thickness of the oxide layer is $h_1^* = 0.1$ μm. The doping profile

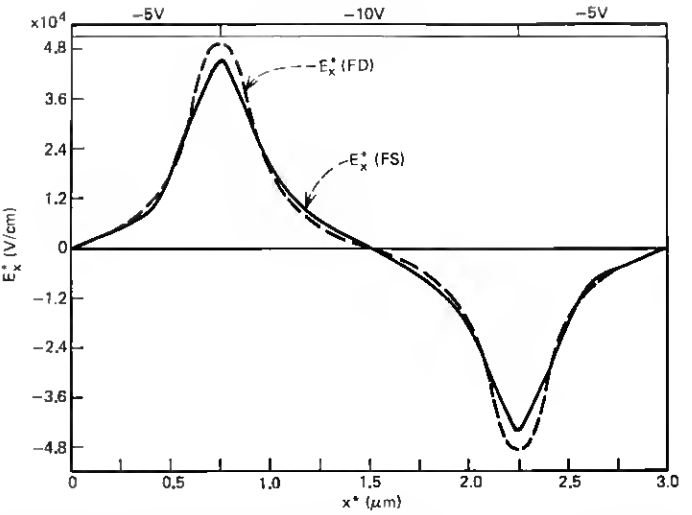

Fig. 10—The field $-(\partial\varphi^*/\partial x^*)(x^*, y^*)$ plotted as a function of x^* in a surface CCD for $y^* = 0.2$ μm. The 1.5-μm plates are alternately at −5 V and −10 V, and the oxide thickness is $h_1^* = 0.2$ μm. The dashed curve is a plot of $-(\partial\varphi^*/\partial x^*)$ for the same device obtained from a finite difference calculation.

in the p-type layer is assumed to be given by eq. (4) with $C_S^* = 4.6 \times 10^{15}/\text{cm}^3$ ($C_S = 46$). This corresponds to an average number density of acceptor atoms of $2 \times 10^{15}/\text{cm}^3$. The remaining physical parameters are as described at the beginning of the section. In Fig. 11 we plot the channel field, $E_x^* = -(\partial\varphi^*/\partial x^*)$, (that is, the field at the potential minimum in the p-region) as a function of x^* for three different p-type layer thicknesses: $h_2^* - h_1^* = 0.1$ μm, 2 μm, and 4 μm. In Fig. 12 we plot the corresponding channel potentials, φ^*, (that is, the value of the potential at the potential minimum in the p-layer). The CCD with $h_2^* - h_1^* = 0.1$ μm is essentially a surface device. As the thickness of the p-layer is increased, the minimum value of the field under the center of the −10-V plate increases at first, while the peak value of the field decreases. Eventually, as the thickness of the p-layer is increased, the channel will be so far below the plates that the channel fields will start decreasing to zero. Thus, in terms of field penetration, there appears to be an optimal p-layer thickness. From Fig. 12, it is clear that as the p-layer gets thicker, the channel potential curve flattens out, and so the charge-carrying capacity of the CCD decreases.

We have also studied the effects of varying the doping in the p-layer (i.e., varying C_S^*). The behavior of the fields is relatively insensitive to changes in C_S^*.

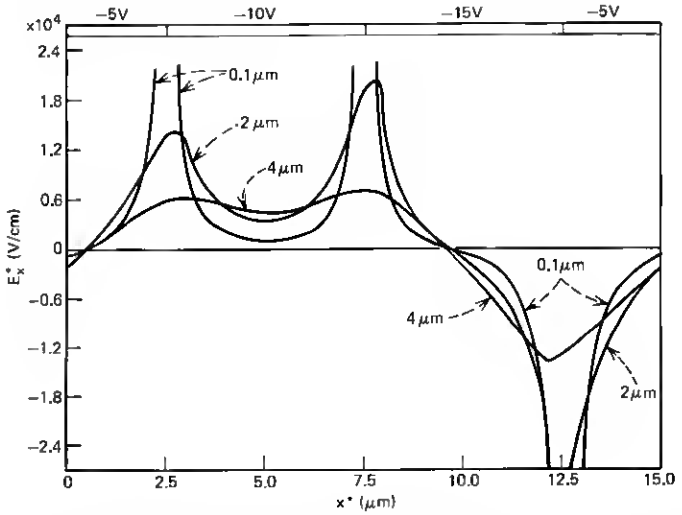

Fig. 11—The channel field $-(\partial\varphi^*/\partial x^*)$ plotted as a function of x^* along the channel for three buried channel CCD's. The 5-μm plates are at -5 V, -10 V, and -15 V, and the oxide thickness is $h_1^* = 0.1$ μm. $C_S^* = 4.6 \times 10^{15}/\text{cm}^3$, and the p-layers are 0.1 μm, 2 μm, and 4 μm thick, respectively.

An operating buried channel CCD has been reported[16] in which the gaps between the plates have been filled with a resistive material so that the potential drop between the plates is essentially linear. The butted plate model can be easily adapted to describe this. In Figs. 13 and 14 we show the channel fields and potentials in such a CCD. This is a three-phase CCD with 10-μm plates and 5-μm gaps. The voltages on the plates are -5 V, -10 V, and -15 V and in the gaps the voltage varies linearly from one plate to the next. The thickness of the oxide layer is $h_1^* = 0.1$ μm. The doping profile in the p-type layer is given by (4) with $C_S^* = 4.6 \times 10^{15}/\text{cm}^3$ ($C_S = 46$). The remaining physical parameters are as described at the beginning of this section. In Fig. 13 we plot the channel field, $E_x^* = -(\partial\varphi^*/\partial x^*)$, as a function of x^* for two different p-layer thicknesses, $h_2^* - h_1^* = 3$ μm and 7 μm. In Fig. 14 we plot the corresponding channel potentials, φ^*. Again, it is seen that the p-layer thickness is a sensitive parameter in terms of field penetration and charge-carrying capacity, and there is undoubtedly an optimal thickness. In Figs. 15 and 16 we plot the same quantities for a three-phase CCD which is identical to the one of Figs. 13 and 14, except that the gap spacing is zero. The devices seem to have essentially the same fields and charge-carrying capacities.

IV. ANALYTIC SOLUTION OF THE LINEARIZED EQUATIONS

In this section we briefly derive the solution of eqs. (21) through (24) subject to the boundary conditions (13) through (15), (17), (25), and (26). We assume as given the Fourier series expansions of $V(x)$ and $Q(x)$:

$$V(x) = \tfrac{1}{2}a_o + \sum_{n=1}^{\infty} (a_n \cos \lambda_n x + b_n \sin \lambda_n x), \tag{29}$$

$$Q(x) = \tfrac{1}{2}\zeta_o + \sum_{n=1}^{\infty} (\zeta_n \cos \lambda_n x + \xi_n \sin \lambda_n x) \tag{30}$$

where

$$\lambda_n = (2n\pi)/L. \tag{31}$$

Since in most cases of interest $V(x)$ and $Q(x)$ are either piecewise constant or linear functions, it is trivial to obtain the coefficients of these series.

Since $\psi(x, y)$ must be periodic in x with period L, we can expand the solution in each of the four regions in a series of the form

$$\psi(x, y) = \tfrac{1}{2}A_o(y) + \sum_{n=1}^{\infty} (A_n(y) \cos \lambda_n x + B_n(y) \sin \lambda_n x). \tag{32}$$

On substituting expressions of the form (32) for ψ into (21) through (24)

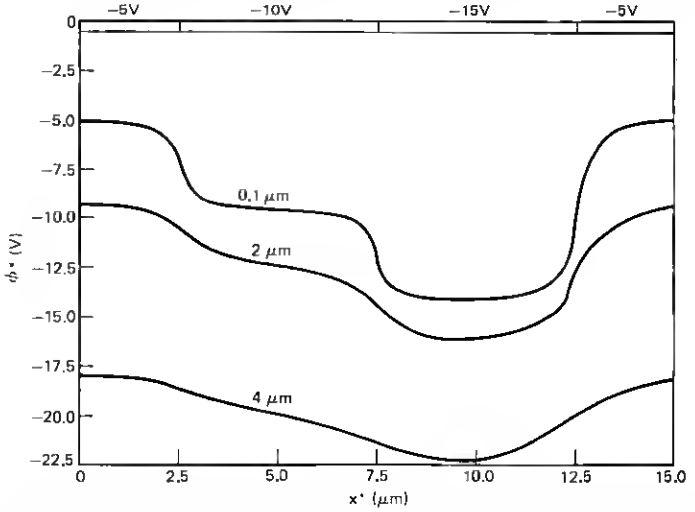

Fig. 12—The channel potential φ^* plotted as a function of x^* along the channel for three buried channel CCD's. The 5-μm plates are at −5 V, −10 V, and −15 V, and the oxide thickness is $h_1 = 0.1$ μm. $C_S^* = 4.6 \times 10^{15}/\text{cm}^3$, and the p-layers are are 0.1 μm, 2 μm, and 4 μm thick, respectively.

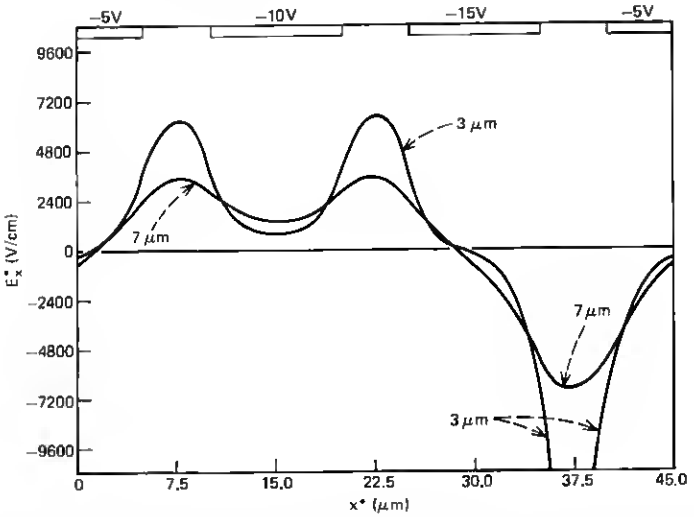

Fig. 13—The channel field $-(\partial\varphi^*/\partial x^*)$ plotted as a function of x^* along the channel for two buried channel CCD's. The 10-μm plates are at -5 V, -10 V, and -15 V and are separated by 5-μm gaps in which the potential varies linearly between plates. $h_1^* = 0.1$ μm, $C_S^* = 4.6 \times 10^{15}/\text{cm}^3$, and the p-layers are 3 μm and 7 μm thick, respectively.

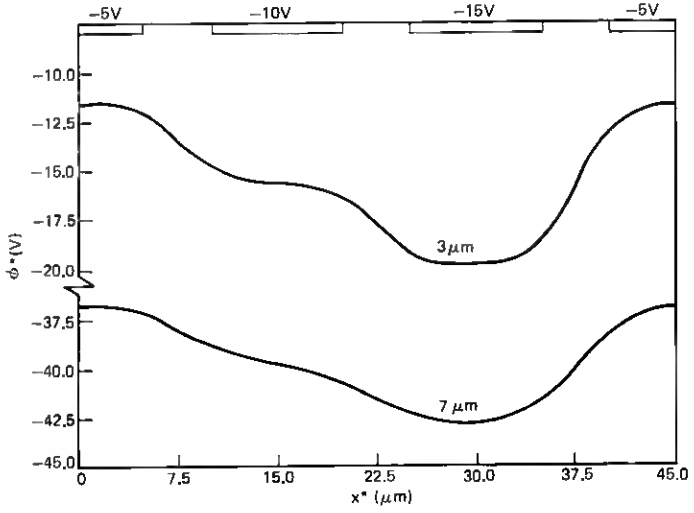

Fig. 14—The channel potential φ^* plotted as a function of x^* along the channel for two buried channel CCD's. The 10-μm plates are at -5 V, -10 V, and -15 V and are separated by 5-μm gaps in which the potential varies linearly between plates. $h_1^* = 0.1$ μm, $C_S^* = 4.6 \times 10^{15}/\text{cm}^3$, and the p-layers are 3 μm and 7 μm thick, respectively.

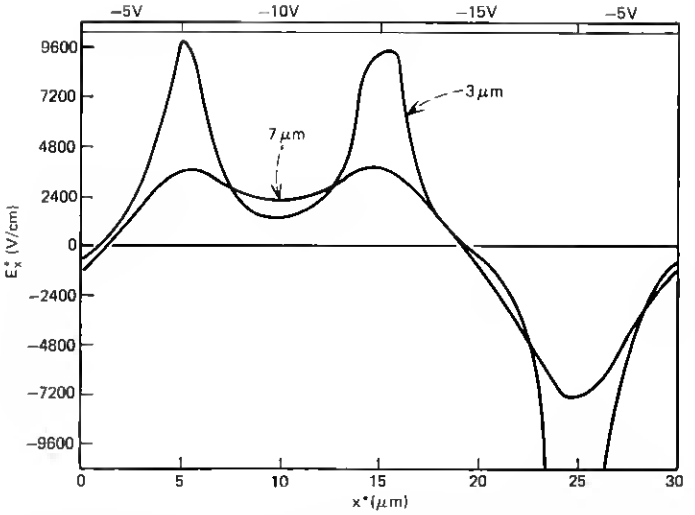

Fig. 15—The channel field $-(\partial\varphi^*/\partial x^*)$ plotted as a function of x^* along the channel for two buried channel CCD's. The 10-μm plates are at -5 V, -10 V, and -15 V, $h_1^* = 0.1$ μm, $C_S^* = 4.6 \times 10^{15}$/cm^3, and the p-layers are 3 μm and 7 μm thick, respectively.

and equating to zero the coefficients of $\cos \lambda_n x$ and $\sin \lambda_n x$, $n = 0, 1, 2, \cdots$, we obtain an uncoupled system of second-order, constant-coefficient, ordinary differential equations from which the $A_n(y)$ and $B_n(y)$ can be determined simply. Each $A_n(y)$ and $B_n(y)$ is the sum of two linearly independent solutions and thus each involves two constants of integration which must be determined by making use of the boundary conditions (13), (14), (15), (17), (25), and (26). Since the Fourier series representing the solutions must be equal term by term at the boundaries, this yields a simple set of linear algebraic equations for the unknown constants of integration. These equations can be solved explicitly, yielding the integration constants as linear functions of the coefficients a_n and b_n, and ζ_n and ξ_n, of the Fourier series for $V(x)$ and $Q(x)$ given in (29) and (30). The algebra involved is elementary but involved, and we only record the final answer here.

Let

$$F_n(x) = a_n \cos \lambda_n x + b_n \sin \lambda_n x, \tag{33}$$

$$\Phi_n(x) = \zeta_n \cos \lambda_n x + \xi_n \sin \lambda_n x, \tag{34}$$

so that we can write

$$V(x) = \tfrac{1}{2} a_o + \sum_{n=1}^{\infty} F_n(x), \tag{35}$$

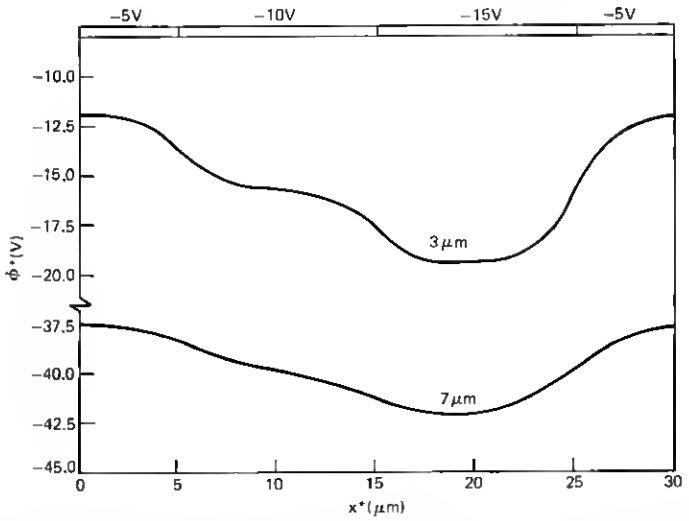

Fig. 16—The channel potential φ^* plotted as a function of x^* along the channel for two buried channel CCD's. The 10-μm plates are at −5 V, −10 V, and −15 V, $h_1^* = 0.1$ μm, $C_S^* = 4.6 \times 10^{15}/\text{cm}^3$, and the p-layers are 3 μm and 7 μm thick, respectively.

$$Q(x) = \tfrac{1}{2}\zeta_o + \sum_{n=1}^{\infty} \Phi_n(x). \tag{36}$$

Furthermore, let

$$E_\pm = 1 \pm 1/\eta, \tag{37}$$

$$\Lambda_n^\pm = 1 \pm (1 + \lambda_n^{-2})^{\frac{1}{2}}, \tag{38}$$

$$M_n(y) = \{E_+ \Lambda_n^+ + E_- \Lambda_n^- e^{-2\lambda_n(h_3-h_1)}\}e^{-\lambda_n y} + \{E_- \Lambda_n^+ e^{-2\lambda_n h_1} + E_+ \Lambda_n^- e^{-2\lambda_n h_3}\}e^{\lambda_n y}, \tag{39}$$

$$L_n(y) = 2\{\Lambda_n^+ e^{-\lambda_n y} + \Lambda_n^- e^{-\lambda_n(2h_3-y)}\}. \tag{40}$$

Then we can write

$$\psi_1(x, y) = (A\bar{a}_o + B) + (C\bar{a}_o + D)y + \sum_{n=1}^{\infty} \left\{ F_n(x) \frac{M_n(y)}{M_n(0)} + \Phi_n(x) \frac{L_n(h_1)}{M_n(0)} \frac{\sinh \lambda_n y}{\eta \lambda_n} \right\}, \tag{41}$$

$$\psi_2(x, y) = \frac{1}{2}\left[\bar{a}_o(1 + h_3 - h_2) - (h_3 - h_2)^2 - (\bar{a}_o + 2h_2 - 2h_3)(y - h_2) + 2\int_{h_2}^{y} (y - \xi)\sigma(\xi)d\xi\right] + \sum_{n=1}^{\infty} \left\{ F_n(x) + \Phi_n(x) \frac{\sinh \lambda_n h_1}{\eta \lambda_n} \right\} \frac{L_n(y)}{M_n(0)}, \tag{42}$$

$$\psi_3(x,y) = \tfrac{1}{2}[\bar{a}_o(1 + h_3 - y) - (y - h_3)^2] + \sum_{n=1}^{\infty} \left\{ F_n(x) + \Phi_n(x) \frac{\sinh \lambda_n h_1}{\eta \lambda_n} \right\} \frac{L_n(y)}{M_n(0)}, \quad (43)$$

$$\psi_4(x, y) = \tfrac{1}{2}\bar{a}_o e^{-(y-h_3)} + 4 \sum_{n=1}^{\infty} \left\{ F_n(x) + \Phi_n(x) \frac{\sinh \lambda_n h_1}{\eta \lambda_n} \right\} \times \frac{\exp[-\sqrt{1 + \lambda_n^2}(y - h_3) - \lambda_n h_3]}{M_n(0)} \quad (44)$$

where

$$A = \frac{1}{2}\left(1 + h_3 - h_1 + \frac{h_1}{\eta}\right), \quad (45)$$

$$B = \int_{h_1}^{h_2} \left(\xi - h_1 + \frac{h_1}{\eta}\right) \sigma(\xi) d\xi - \frac{1}{2}\left[(h_3 - h_2)(h_3 + h_2 - 2h_1) + \frac{h_1}{\eta}(\zeta_o + 2h_3 - 2h_2)\right], \quad (46)$$

$$C = -1/(2\eta), \quad (47)$$

$$D = \left[\zeta_o + 2(h_3 - h_2) - 2\int_{h_1}^{h_2} \sigma(\xi) d\xi\right] \Big/ (2\eta), \quad (48)$$

and

$$\bar{a}_o = (\tfrac{1}{2}a_o - B)/A. \quad (49)$$

Equations for $\partial\psi/\partial x$ and $\partial\psi/\partial y$ can be obtained by differentiating eqs. (41) through (44) term by term. To obtain the equations for a surface CCD, drop equation (42) and set $\sigma = 0$, $h_2 = h_1$, and relabel h_3, ψ_3, and ψ_4 as h_2, ψ_2, and ψ_3 in the remaining equations.

V. FINITE DIFFERENCE SOLUTION OF THE EXACT EQUATIONS

In this section we describe the finite difference (FD) solution[17] of a surface CCD described by equations (10) through (17). We will assume that $Q(x) \equiv 0$, $\sigma(y) \equiv 0$, and $h_1 = h_2 = h$.

The infinite region $0 \leqq x \leqq L$, $h \leqq y < \infty$ is replaced by the finite rectangle $0 \leqq x \leqq L$, $h \leqq y \leqq H$, with $H \gg h$, and the boundary condition (16) is replaced for $0 \leqq x \leqq L$ by

$$\varphi_2(x, H) = 0. \quad (50)$$

This may be done, because the solution tends to zero rapidly as $y \to \infty$. In fact, a one-dimensional analysis[5] shows that φ_2 tends to zero exponentially in y.

A uniform FD net is now placed over region 1 (the oxide layer) and

region 2 (the silicon layer) with N points in the x-direction and M_1 and M_2 points in the y-direction in regions 1 and 2, respectively. Let

$$\begin{aligned} h_x &= L/(N-1), \qquad h_{1y} = h/(M_1-1), \\ h_{2y} &= (H-h)/(M_2-1), \end{aligned} \tag{51}$$

and then, for $(1 \leqq i \leqq N)$, $(1 \leqq j \leqq M_\alpha)$, and $(\alpha = 1, 2)$, define

$$\varphi_{\alpha,i,j} = \varphi_\alpha((i-1)h_x, (j-1)h_{\alpha y}) \tag{52}$$

where $\varphi_\alpha(x,y)$ is the exact solution of (10) through (17), and define $\hat{\varphi}_{\alpha,i,j}$ as the FD solution which approximates $\varphi_{\alpha,i,j}$.

The FD equations are obtained as follows. The boundary condition (50) is replaced by the N equations

$$\hat{\varphi}_{2,i,M_2} = 0, \qquad (1 \leqq i \leqq N), \tag{53}$$

while the boundary condition (13) is replaced by the N equations

$$\hat{\varphi}_{1,i,1} = V((i-1)h_x) = V_i, \qquad (1 \leqq i \leqq N). \tag{54}$$

If $x_o = (i_o - 1)h_x$ is the edge of a plate, the jump discontinuity in $V(x)$ there is handled by setting

$$V_{i_o} = \tfrac{1}{2}(V_{i_o+1} + V_{i_o-1}). \tag{55}$$

At each interior mesh point $\nabla^2\varphi_{\alpha,i,j}$ is approximated by the standard five-point difference formula[17]

$$\begin{aligned} \nabla_h^2\hat{\varphi}_{\alpha,i,j} = {} & (\hat{\varphi}_{\alpha,i+1,j} + \hat{\varphi}_{\alpha,i-1,j} - 2\hat{\varphi}_{\alpha,i,j})/h_x^2 \\ & + (\hat{\varphi}_{\alpha,i,j+1} + \hat{\varphi}_{\alpha,i,j-1} - 2\hat{\varphi}_{\alpha,i,j})/h_{\alpha y}^2. \end{aligned} \tag{56}$$

Equation (56) can also be used to evaluate $\nabla_h^2\hat{\varphi}_{\alpha,1,j}$ and $\nabla_h^2\hat{\varphi}_{\alpha,N,j}$, $(2 \leqq j \leqq M_\alpha - 1)$ by making use of the periodicity relations

$$\hat{\varphi}_{\alpha,-1,j} = \hat{\varphi}_{\alpha,N-1,j}, \qquad \hat{\varphi}_{\alpha,N+1,j} = \hat{\varphi}_{\alpha,1,j}. \tag{57}$$

Thus, eqs. (10) and (12) are replaced by $(M_1 + M_2 - 4)N$ equations

$$\nabla_h^2\hat{\varphi}_{1,i,j} = 0, \qquad (1 \leqq i \leqq N), \qquad (2 \leqq j \leqq M_1 - 1), \tag{58}$$

$$\nabla_h^2\hat{\varphi}_{2,i,j} = \exp(\hat{\varphi}_{2,i,j}) - 1, \qquad (1 \leqq i \leqq N), \quad (2 \leqq j \leqq M_2 - 1). \tag{59}$$

There remain the interface conditions (14). The first of these is replaced by the N equations

$$\hat{\varphi}_{1,i,M_1} = \hat{\varphi}_{2,i,1}, \qquad (1 \leqq i \leqq N). \tag{60}$$

To obtain an equivalent set of equations for the second condition, we could replace the derivatives by the first differences from each side.

However, it is well known that this approximation is not very good. This is easily seen from the prototype equation $\nabla^2\varphi = 0$, where, for simplicity, we take $h_x = h_y = h$. Then as is well known,[17]

$$\varphi_{i+1,j} + \varphi_{i-1,j} + \varphi_{i,j+1} + \varphi_{i,j-1} - 4\varphi_{i,j} = h^2\nabla^2\varphi_{ij} + 0(h^4), \quad (61)$$

while

$$\varphi_{i,j+1} - \varphi_{i,j} = h\frac{\partial\varphi}{\partial y}(x_i, y_j) + 0(h^2). \quad (62)$$

Thus, the errors in the FD equations, after scaling the left-hand sides to have coefficients of order 1, are out of balance. The interface condition is $1/h^2$ less accurately modeled than the differential equation. This leads to the following scheme which balances the errors equally. We want $\partial\varphi_1/\partial y$ using only values of φ_1, similarly for $\partial\varphi_2/\partial y$, and the approximation must be good to $0(h^3)$. This may be done using the values of $\varphi_{1,i,j}$, $(M_1 - 3 \leqq j \leqq M_1)$. Simply use the derivative of the cubic interpolation polynomial through these values. It is easily seen that

$$\frac{\partial\varphi_1}{\partial y}(x_i, h) = \{11\varphi_{1,i,M_1} - 18\varphi_{1,i,M_1-1} + 9\varphi_{1,i,M_1-2} - 2\varphi_{1,i,M_1-3}\}/(6h_{1y}) + 0(h_{1y}^3). \quad (63)$$

Similarly,

$$\frac{\partial\varphi_2}{\partial y}(x_i, h) = \{2\varphi_{2,i,4} - 9\varphi_{2,i,3} + 18\varphi_{2,i,2} - 11\varphi_{2,i,1}\}/(6h_{2y}) + 0(h_{2y}^3). \quad (64)$$

Then the second boundary condition (14) is replaced by the N equations

$$\eta\{11\hat{\varphi}_{1,i,M_1} - 18\hat{\varphi}_{1,i,M_1-1} + 9\hat{\varphi}_{1,i,M_1-2} - 2\hat{\varphi}_{1,i,M_1-3}\}/h_{1y} = \{2\hat{\varphi}_{2,i,4} - 9\hat{\varphi}_{2,i,3} + 18\hat{\varphi}_{2,i,2} - 11\hat{\varphi}_{2,i,1}\}/h_{2y}, \quad (1 \leqq i \leqq N). \quad (65)$$

Equations (53), (54), (58), (59), (60), and (65) comprise $(M_1 + M_2)N$ equations in the $(M_1 + M_2)N$ unknowns $\hat{\varphi}_{\alpha,i,j}$, $(\alpha = 1, 2)$, $(1 \leqq i \leqq N)$, and $(1 \leqq j \leqq M_\alpha)$. From the standard FD theory, the solution of this set of transcendental equations differs from the solution of the true boundary value problem by a factor of order $0(h^2)$. We used a nonlinear overrelaxation scheme developed in Refs. 18 through 20 to solve the FD equations for $\hat{\varphi}_2$ and standard overrelaxation methods[21] to solve the $\hat{\varphi}_1$ FD equations.

An initial estimate of the solution, $\hat{\varphi}^{(0)}_{\alpha,i,j}$, was obtained by computing the one-dimensional matching solutions as functions of y along the

lines $x = x_i$, $(1 \leqq i \leqq N)$, using the methods of Ref. 5. This provides a solution which is a fairly good estimate under the middle of any plate and a very bad one near the edge of any plate. These one-dimensional solutions also give a good estimate of the greatest depth of the transition region, call it $y_{\max}$. Since $\varphi_2 \to 0$ exponentially for $y > y_{\max}$, we chose $H = y_{\max} + 20$.

This estimated solution $\hat{\varphi}^{(0)}_{\alpha,i,j}$ is now refined iteratively by the method of successive overrelaxation (SOR). The $(n+1)$st iterate is obtained from the nth as follows. For all $n = 0, 1, 2, \cdots$, set

$$\hat{\varphi}^{(n)}_{1,i,1} = V_i, \qquad \hat{\varphi}^{(n)}_{2,i,M_2} = 0, \qquad (1 \leqq i \leqq N). \tag{66}$$

For $(2 \leqq i \leqq N-1)$ and $(2 \leqq j \leqq M_1 - 1)$, let $\tilde{\varphi}^{(n+1)}_{1,i,j}$ be defined by

$$(2h_x^{-2} + 2h_{1y}^{-2})\,\tilde{\varphi}^{(n+1)}_{1,i,j} = (\hat{\varphi}^{(n)}_{1,i+1,j} + \hat{\varphi}^{(n+1)}_{1,i-1,j})h_x^{-2} + (\hat{\varphi}^{(n)}_{1,i,j+1} + \varphi^{(n+1)}_{1,i,j-1})h_{1y}^{-2}. \tag{67}$$

Then set

$$\hat{\varphi}^{(n+1)}_{1,i,j} = \omega_1\,\tilde{\varphi}^{(n+1)}_{1,i,j} + (1 - \omega_1)\,\hat{\varphi}^{(n)}_{1,i,j} \tag{68}$$

where ω_1 is an overrelaxation parameter satisfying $1 \leqq \omega_1 < 2$. For $(2 \leqq i \leqq N-1)$ and $(2 \leqq j \leqq M_2 - 1)$, let $\tilde{\varphi}_{2,i,j}$ be the solution of

$$(2h_x^{-2} + 2h_{2y}^{-2})\,\tilde{\varphi}^{(n+1)}_{2,i,j} + \exp(\tilde{\varphi}^{(n+1)}_{2,i,j}) = 1 + (\hat{\varphi}^{(n)}_{2,i+1,j} + \hat{\varphi}^{(n+1)}_{2,i-1,j})h_x^{-2} + (\hat{\varphi}^{(n)}_{2,i,j+1} + \hat{\varphi}^{(n+1)}_{2,i,j-1})h_{2y}^{-2}. \tag{69}$$

Equation (69) has the form

$$Aw + e^w = B \tag{70}$$

where A and B are known and $A > 0$. Given any approximate solution w^0 of (70), Newton's method[22] yields the sequence

$$w^{k+1} = [A + e^{w^k}]^{-1}[B + (w^k - 1)e^{w^k}], \qquad (k = 0, 1, 2, \cdots), \tag{71}$$

which converges to the solution of (69). The convergence of this scheme is global and quadratic because the function $Aw + e^w$, for $A > 0$, is a monotone increasing, convex function of w. After solving for $\tilde{\varphi}^{(n+1)}_{2,i,j}$, we set

$$\hat{\varphi}^{(n+1)}_{2,i,j} = \omega_2\,\tilde{\varphi}^{(n+1)}_{2,i,j} + (1 - \omega_2)\,\hat{\varphi}^{(n)}_{2,i,j} \tag{72}$$

where $1 \leqq \omega_2 < 2$.

The interface values $\hat{\varphi}_{1,i,M_1}$ and $\hat{\varphi}_{2,i,1}$, $(2 \leqq i \leqq N-1)$ are relaxed by combining (60) and (65), defining

$$\tilde{\varphi}^{(n+1)}_{1,i,M_1} = \tilde{\varphi}^{(n+1)}_{2,i,1} = (\eta h_{1y}^{-1} + h_{2y}^{-1})^{-1}[\eta h_{1y}^{-1}(18\hat{\varphi}^{(n+1)}_{1,i,M_1-1} - 9\hat{\varphi}^{(n+1)}_{1,i,M_1-2} + 2\hat{\varphi}^{(n+1)}_{1,i,M_1-1}) + h_{2y}^{-1}(18\hat{\varphi}^{(n)}_{2,i,2} - 9\hat{\varphi}^{(n)}_{2,i,3} + 2\hat{\varphi}^{(n)}_{2,i,4})]/(11), \tag{73}$$

and setting

$$\hat{\varphi}_{1,i,M_1}^{(n+1)} = \hat{\varphi}_{2,i,1}^{(n+1)} = \omega \tilde{\varphi}_{1,i,M_1}^{(n+1)} + (1 - \omega)\hat{\varphi}_{1,i,M_1}^{(n)} \tag{74}$$

where

$$\omega = \tfrac{1}{2}(\omega_1 + \omega_2). \tag{75}$$

Equations (66) through (75) describe the manner in which the interior nodes of the FD mesh are relaxed. The nodes at $i = 1$ and N involve periodicity and require more detailed study. By using the periodicity relations (57), equations (66) through (75) can be extended to the nodes at $i = 1, N$. We could next do one of two things. First, we could treat $\hat{\varphi}_{\alpha,1,j}$ and $\hat{\varphi}_{\alpha,N,j}$ as separate quantities and relax each of them separately using the periodicity relations (57). Then, each time $\hat{\varphi}_{\alpha,1,j}$ was relaxed, this new value could be substituted for $\hat{\varphi}_{\alpha,N,j}$ to preserve periodicity, and vice versa. This was tried but gave very poor convergence rates. The problem is that in treating $\hat{\varphi}_{\alpha,1,j}$ and $\hat{\varphi}_{\alpha,N,j}$ as separate quantities, the same quantity (that is $\hat{\varphi}_{\alpha,1,j}$ and $\hat{\varphi}_{\alpha,N,j}$) gets relaxed twice rather than once in each SOR sweep. This can be avoided by letting $\hat{\varphi}_{\alpha,N,j} \equiv \hat{\varphi}_{\alpha,1,j}$, $(\alpha = 1, 2)$, $(2 \leqq j \leqq M_\alpha - 1)$ and then relaxing only the quantities $\hat{\varphi}_{\alpha,1,j}$. This produces quite acceptable convergence rates.

The overrelaxation parameters ω_1 and ω_2 were set equal to the optimum values of these parameters for the Laplace equation on regions one and two respectively. These values for ω_1 and ω_2 were estimated as follows. Let $\hat{\boldsymbol{\varphi}}_\alpha^{(n)}$ denote the vector of values of the nth iterate of the solution to $\nabla_h^2 \hat{\varphi}_\alpha = 0$ in region α, $(\alpha = 1, 2)$. Define the nth residual vector as $\mathbf{R}_\alpha^{(n)} = \hat{\boldsymbol{\varphi}}_\alpha^{(n+1)} - \hat{\boldsymbol{\varphi}}_\alpha^{(n)}$. Then, starting with any initial guess $\hat{\boldsymbol{\varphi}}_\alpha^{(0)} \not\equiv 0$, standard theory shows[23] that $\lim_{n \to \infty} \|\mathbf{R}_\alpha^{(n+1)}\| / \|\mathbf{R}_\alpha^{(n)}\| = \eta_\alpha$ exists and

$$\omega_{\alpha,\text{opt}} = 2/\{1 + \sqrt{1 - \eta_\alpha}\} \tag{76}$$

where $\|\mathbf{R}_\alpha^{(n)}\|$ denotes the norm of the vector $\mathbf{R}_\alpha^{(n)}$ and is called the residual. In practice, we calculated the residuals for n large enough so that η_α was obtained to the desired accuracy using the L_2 norm.

A further important point is solving the transcendental equation (69), which must be done at each SOR step. In the $(n + 1)$th SOR sweep, the initial estimate for $\tilde{\varphi}_{2,i,j}^{(n+1)}$ in the Newton iteration (71) was $\hat{\varphi}_{2,i,j}^{(n)}$. There is no reason to compute the $\tilde{\varphi}_{2,i,j}^{(n+1)}$ very accurately when $\hat{\varphi}_{2,i,j}^{(n)}$ is far away from its final value. Conversely, the quadratic convergence of Newton's method means that when the error in $\hat{\varphi}_{2,i,j}^{(n)}$ is small, one Newton iteration will produce a very good approximation for $\tilde{\varphi}_{2,i,j}^{(n+1)}$. For this reason, only one Newton iteration was used in solving (69) during each SOR sweep.

Some theory has been developed to show that the SOR scheme we have outlined above converges to the true solution in some mildly nonlinear Dirichlet problems.[18,19] However, to the best of our knowledge, no theoretical analysis exists of the boundary value problem of this paper. Nevertheless, as we will demonstrate by numerical examples in the next section, the scheme works in practice.

We conclude this section with a few remarks on the estimated accuracy of the FD solution. Since little is known of the general theory of a complicated nonlinear boundary value problem such as we are considering, we argue by analogy with the Dirichlet problem for Laplace's equation on a square. Let $\varphi(x, y)$ be the true solution of $\nabla^2\varphi = 0$ in $0 < x, y < L$, with φ specified on the boundary, let $h = L/(N-1)$, $\varphi_{i,j} = \varphi((i-1)h, (j-1)h)$, and let $\hat{\varphi}_{ij}$ be the solution of the corresponding FD equations. Then it is well known[24] that under reasonable conditions on the boundary values,

$$\|\varphi - \hat{\varphi}\|_\infty = \sup_{1 \leqq i,\, j \leqq N} |\varphi_{ij} - \hat{\varphi}_{ij}| = \mathbf{0}(h^2). \tag{77}$$

This relationship assumes that we know the FD solution exactly. However, we don't know $\hat{\varphi}$ exactly, all we know are the various iterates $\hat{\varphi}^{(n)}$ which have been calculated and the residuals $\|\hat{\varphi}^{(n+1)} - \hat{\varphi}^{(n)}\|_\infty$. Now it is known, though not as widely as it should be, when calculating $\hat{\varphi}$ by the method of SOR that[25]

$$\|\hat{\varphi} - \hat{\varphi}^{(n+1)}\|_\infty = C(\omega)\|\hat{\varphi}^{(n+1)} - \hat{\varphi}^{(n)}\|_\infty, \tag{78}$$

and if ω_b is the optimal choice of ω,

$$C(\omega_b) = 0(N). \tag{79}$$

It can also be shown, if the optimal value of ω is underestimated by ten or fifteen percent, that $C(\omega) = 0(N^2)$. This means that to obtain an approximate solution accurate to $0(h^2) = 0(N^{-2})$ by the method of SOR, we must iterate at least until the residuals are $0(N^{-3})$, and since in the nonlinear problem we can only crudely estimate the optimal ω, we should really iterate until the residuals are $0(N^{-4})$.

As we will show by example in the next section, it is necessary to calculate the potentials with great accuracy if one wishes to obtain the fields from them with any accuracy at all by differencing them. From the previous paragraph, however, we have shown that this is expensive in even a moderately complicated problem, since then the residuals must be made so small. To estimate the cost of increasing the size of the problem or decreasing the mesh size (both equivalent to increasing N),

we note that typically in SOR,[26]

$$\|\hat{\varphi}^{(n+1)} - \hat{\varphi}^{(n)}\|_\infty \approx e^{-n|0(N^{-1})|} \tag{80}$$

for optimal ω, while for nonoptimal ω,

$$\|\hat{\varphi}^{(n+1)} - \hat{\varphi}^{(n)}\|_\infty \approx e^{-n|0(N^{-2})|}. \tag{81}$$

If we wish to specify that $\|\hat{\varphi} - \hat{\varphi}^{(n+1)}\|_\infty \leqq \epsilon$, then, for optimal ω, it is easy to show from (78) through (80) that the number of iterations must be

$$n = 0(N\,\ell n(N/\epsilon)), \tag{82}$$

while for nonoptimal ω, it follows from (78), (79), and (81) that

$$n = 0(N^2 \ell n(N/\epsilon)). \tag{83}$$

Thus, if we decrease the mesh size by one half, then from (82) or (83), we must double or quadruple the number of iterations to obtain the same accuracy. Since there are now 4 times as many mesh points, the time required to obtain a solution goes up by a factor of 8 or 16, depending on the knowledge of ω.

VI. COMMENTS ON THE ACCURACY OF THE SOLUTIONS

In Section IV we derived the Fourier series solution (FSS) of the linearized problem, and in Section V we outlined the finite difference solution (FDS) of the nonlinear problem. In this section we compare several of these solutions with regard to accuracy and cost. All calculations discussed were performed on a Honeywell 6070 computer, and all programs were written in Fortran IV.

We solved the nonlinear equations (10) through (17) by the method of finite differences for the two-phase surface CCD's discussed in Section III, some of whose properties are presented graphically in Figs. 5 through 10. The three CCD's have plate widths of 45 μm, 5 μm, and 1.5 μm, respectively. The plate voltages are -5 V and -10 V, $Q(x) \equiv 0$, $N_D = 10^{14}/\text{cm}^3$, $\epsilon_1/\epsilon_0 = 4$, $\epsilon_2/\epsilon_0 = 12$, and $\lambda_D = 0.415$ μm. In all cases, a FD net was chosen with $N = 25$, $M_1 = 25$, and $M_2 = 41$.

In the case of the 45-μm-plate device, this corresponds in the dimensionless units to $h_x = 9$, $h_{1y} = 0.02$, $h_{2y} = 1$. After 273 SOR iterations, the residual was $\sim 4 \times 10^{-7}$, the running time was 195 seconds, and 35 K of memory was used. This should ensure that the difference between the true FDS and the iterated solution will never exceed $\sim 25 \times 65 \times 4 \times 10^{-7} = 6.5 \times 10^{-4}$. We have calculated the FSS at the same mesh points, this took 33 seconds to run, and 33 K of memory

was used. Let $\varphi_{FD}(x, y)$ denote the FD solution of the nonlinear problem and $\psi(x, y)$ denote the FS solution of the linearized problem, and

$$e(x, y) = |(\varphi_{FD}(x, y) - \psi(x, y))/\varphi_{FD}(x, y)|. \tag{84}$$

Then we found that along the oxide-semiconductor interface, $e(x, h_1) < 1.14 \times 10^{-2}$, $0 \leqq x \leqq L$, and five Debye lengths below this interface, $e(x, h_1 + 5) < 2.89 \times 10^{-2}$, $0 \leqq x \leqq L$

We have for the 5-μm-plate device $h_x = 1$, $h_{1y} = 0.02$, $h_{2y} = 1$. After 288 SOR iterations, the residual was $\sim 4 \times 10^{-7}$, the running time was 190 seconds, and 35 K of memory was used. This should again ensure that the difference between the true FDS and the iterated solution does not exceed 6.5×10^{-4}. For this case, we found that $e(x, h_1) < 2.8 \times 10^{-3}$, $e(x, h_1 + 5) < 1.4 \times 10^{-3}$, $e(x, h_1 + 10) < 3.14 \times 10^{-3}$, $e(x, h_1 + 15) < 9.81 + 10^{-3}$ for $0 \leqq x \leqq L$. The running time to evaluate the FSS was 10 seconds and 33 K of memory was used.

Finally, for the 1.5-μm-plate device, we have $h_x = 0.3$, $h_{1y} = 0.02$, and $h_{2y} = 1$. After 300 SOR iterations the residual was $\sim 6 \times 10^{-4}$, the running time was 196 seconds, and 35 K of memory was used. Note that in this case the residual is three orders of magnitude greater than in the other two cases. We found that $e(x, h_1) < 1.8 \times 10^{-2}$, the running time to calculate the FSS was 4 seconds, and 33 K of memory was used.

In Ref. 5 it was noted that as long as $|\psi_4(h_3) + 1| < 10$, one could expect the solution of the linearized problem to be a good approximation to the solution of the nonlinear problem, at least in the p-region for buried channel devices or near the oxide-semiconductor interface for surface devices. In the examples considered here, for the 45-μm-plate case, $-5.15 < \psi_4(x, h_3) < 3.00$, for the 5-$\mu$m-plate device, $-1.20 < \psi_4(x, h_3) < -0.96$, and for the 1.5-$\mu$m-plate case, $\psi_4(x, h_3) \equiv -1.077$. This again suggests that the smaller $|\psi_4(x, h_3) + 1|$, the more accurate the approximation.

These examples show that if one only needs a knowledge of the potential in the neighborhood of the oxide-semiconductor interface, the FSS provides a highly accurate approximation to the true solution much more cheaply than can be obtained by FD methods. In fact, to analyze three-phase devices, the cost of obtaining a FDS goes up sharply while the cost of a FSS remains nominal. For example, it took only 15 seconds and 34 K of memory to obtain the solutions presented graphically in Figs. 15 and 16.

In reality, we are as much interested in the fields as we are in the potentials, and it is at this point that the difficulty with using the FD

method for solving these problems becomes most acute. In Figs. 6, 8, and 10, the dashed curves are plots of $-(\partial \varphi_{FD}/\partial x)$ along $y = h_1$, obtained from the FDS just discussed by differencing. In Fig. 6 for example, the two curves differ by nearly an order of magnitude at their peaks. If we take the FSS and difference it to estimate the first derivative, we get a result which, in the neighborhood of the peaks, differs by at most 3 percent from the derivative obtained by differencing the FDS. We can conclude that the fields obtained from the FDS are badly in error. In order to calculate the fields from the FDS with any degree of accuracy, even for these simple examples, we would have to take a mesh so fine that the cost would become prohibitive.

VII. ACKNOWLEDGMENTS

The authors would like to thank G. E. Smith for originally suggesting this research and for many subsequent conversations. They are also indebted to R. H. Krambeck, R. J. Strain, and R. H. Walden for many fruitful conversations on CCD's.

REFERENCES

1. Boyle, W. S., and Smith, G. E., "Charge Coupled Semiconductor Devices," B.S.T.J., *49*, No. 4 (April 1970), pp. 587–593.
2. Amelio, G. F., Tompsett, M. F., and Smith, G. E., "Experimental Verification of the Charge Coupled Device Concept," B.S.T.J., *49*, No. 4 (April 1970), pp. 593–600.
3. Strain, R. J., and Schryer, N. L., "A Nonlinear Diffusion Analysis of Charge-Coupled-Device Transfer," B.S.T.J., *50*, No. 6 (July–August 1971), pp. 1721–1740.
4. Amelio, G. F., "Computer Modeling of Charge-Coupled Device Characteristics," B.S.T.J., *51*, No. 3 (March 1972), pp. 705–730.
5. McKenna, J., and Schryer, N. L., "On the Accuracy of the Depletion Layer Approximation for Charge Coupled Devices," B.S.T.J., *51*, No. 7 (September 1972), pp. 1471–1485.
6. McKenna, J., and Schryer, N. L., unpublished work.
7. Walden, R. H., Krambeck, R. H., Strain, R. J., McKenna, J., Schryer, N. L., and Smith, G. E., "The Buried Channel Charge Coupled Device," B.S.T.J., *51*, No. 7 (September 1972), pp. 1635–1640.
8. Boyle, W. S., and Smith, G. E., "Charge-Coupled Devices–A New Approach to MIS Device Structures," IEEE Spectrum, *8*, No. 7 (July 1971), pp. 18–27.
9. Engeler, W. C., Tiemann, J. J., and Baertsch, R. D., "Surface Charge Transport in Silicon," Appl. Phys. Lett., *17*, No. 11 (December 1970), pp. 469–472.
10. Berglund, C. N., Powell, R. J., Nicollian, E. H., and Clemens, J. T., "Two-Phase Stepped Oxide CCD Shift Register Using Undercut Isolation," Appl. Phys. Lett., *20*, No. 11 (June 1972), pp. 412–414.
11. Lewis, J. A., McKenna, J., and Wasserstrom, E., "Field of Negative Point, Line or Plane Charges in an n-Type Semiconductor," J. Appl. Phys., *41*, No. 10 (September 1970), pp. 4182–4189.
12. Grove, A. S., *Physics and Technology of Semiconductor Devices*, New York: John Wiley & Sons, 1967, pp. 49–50.
13. Abramowitz, M., and Stegun, I. A., *Handbook of Mathematical Functions*, Washington, D. C.: National Bureau of Standards, 1964, p. 297.

14. Krambeck, R. H., Walden, R. H., and Pickar, K. A., "Implanted-Barrier Two-Phase Charge-Coupled Device," Appl. Phys. Lett., *19*, No. 12 (December 1971), pp. 520–522.
15. Tompsett, M. F., "The Quantitative Effects of Interface States on the Performance of Charge-Coupled Devices," IEEE Trans. Elec. Devices, *ED-12*, No. 1 (January 1973), pp. 45–55.
16. Elson, B. M., "Charge-Coupled Concept Studied for Photo-Sensors," Aviation Week & Space Technology, *96*, No. 21 (May 22, 1972), pp. 73–75.
17. Varga, R. S., *Matrix Iterative Analysis*, Englewood Cliffs, N.J.: Prentice-Hall, 1962, chapter 6.
18. Bers, L., "On Mildly Nonlinear Partial Difference Equations of Elliptic Type," J. Res. Nat. Bur. Standards, *51*, No. 11 (November 1953), pp. 229–236.
19. Ortega, J. M., and Rockoff, M. L., "Nonlinear Difference Equations and Gauss-Seidel Type Iterative Methods," SIAM J. Numer. Anal., *3*, No. 9 (September 1966), pp. 497–513.
20. Wasserstrom, E., and McKenna, J., "The Potential Due to a Charged Metallic Strip on a Semiconductor Surface," B.S.T.J., *49*, No. 5 (May–June 1970), pp. 853–877.
21. Varga, R. S., op. cit., chapter 4.
22. Hamming, R. W., *Numerical Methods for Scientists and Engineers*, New York: McGraw-Hill, 1962, p. 81.
23. Forsythe, G. E., and Wasow, W. R., *Finite Difference Methods for Partial Differential Equations*, New York: John Wiley & Sons, 1960, p. 257.
24. Ibid, section 23.
25. Weinberger, H. F., "A Posteriori Error Bounds in Iterative Matrix Inversion," in *Numerical Solution of Partial Differential Equations* (Proc. Symp. Univ. Maryland, 1965), ed. J. H. Bramble, New York: Academic Press, 1966, pp. 153–163.
26. Varga, R. S., op. cit., p. 204.